

Saclay-T96/133

25 November 1996

Damping rates of hard momentum particles in a cold ultrarelativistic plasma

Benoît Vanderheyden

Department of Physics, University of Illinois at Urbana-Champaign, Urbana, IL 61801

Jean-Yves Ollitrault*

Service de Physique Théorique[†], CE-Saclay, 91191 Gif-sur-Yvette, Cedex, France

(December 2, 2024)

Abstract

We compute the damping rates of one-particle excitations in a cold ultrarelativistic plasma to leading order in the coupling constant e for three types of interaction: Yukawa coupling to a massless scalar boson, QED and QCD. Damping rates are of order $e^3\mu$, $e^4\mu$ or $e^4\mu \log(1/e)$. In particular, we find that the damping rate of an electron or of a quark is constant far from the Fermi surface, while it decreases linearly with the excitation energy close to the Fermi surface due to the long-range magnetic interaction.

*Affiliated with CNRS

[†]Laboratoire de la Direction des Sciences de la Matière du Commissariat à l'Energie Atomique

I. INTRODUCTION

The study of ultrarelativistic QED and QCD plasmas has received much attention in the last ten years (for a review, see [1]). This interest has been stimulated by the experimental search for the quark–gluon plasma in high energy heavy ion collisions, and also by theoretical difficulties encountered in the calculation of various physical quantities, many of which are infrared divergent when evaluated to leading order in naive perturbation theory [2–8]. Some of these infrared divergences, such as those appearing in the calculation of the energy loss of a heavy fermion [9] or of the transport coefficients of the plasma [10], are cured by taking into account collective screening phenomena. A major step has been the development by Braaten and Pisarski of a modified perturbation theory involving resummed propagators and vertices which properly describe these collective excitations and their interactions [11]. An equivalent formulation has been given in terms of kinetic theory and mean fields, in which the physical phenomena at work appear clearly [12]. However, even in the frame of this modified perturbation theory, logarithmic infrared divergences remain in the calculation of the fermion damping rate at high temperature [4–6]; this problem has been solved only recently [13].

Most works have been devoted to plasmas with zero chemical potential, i.e. having as many electrons as positrons (resp. as many quarks and antiquarks) for QED (resp. QCD), in order to focus on the difficulties associated with finite temperature. We study here the opposite case, namely a plasma with high chemical potential and zero temperature. Collective excitations are still present in such a system; furthermore, they have the same spectra and screening properties to leading order in e as at high temperature [14], hence the modified perturbation theory of Braaten and Pisarski can still be used [15]. But in contrast to the high temperature case, damping rates of excitations are finite and can be calculated directly, which is the purpose of the present work.

We study a system of fermions in its lowest energy state, i.e. a degenerate Fermi sea at zero temperature. We assume that the ground state has a well-defined Fermi surface.

Since we are interested in the ultrarelativistic limit, the fermion mass is set equal to zero throughout the paper. Then, in the limit of infinite volume, the only energy scale in the system is the chemical potential μ , i.e. the Fermi energy.

Three types of interaction lagrangians are considered. This will help us to understand the features which are specific to gauge theories: (1) a Yukawa interaction mediated by a massless scalar field ϕ , $\mathcal{L}_Y = e\bar{\psi}\psi\phi$; (2) electromagnetic interaction $\mathcal{L}_{QED} = e\bar{\psi}\gamma_\mu\psi A^\mu$; (3) non-abelian $SU(N_c)$ interaction. The coupling constant is assumed to be much smaller than unity, $e \ll 1$, to ensure that a perturbative expansion in powers of e is reliable. Throughout the paper, we use the generic names bosons (b), fermions (f) and antifermions (\bar{f}) when discussing features which are common to these three theories.

One-particle excitations of the Fermi sea are obtained by adding or removing one particle from the ground state. Four types of excitations can be distinguished: (1) one fermion is added above the Fermi level (fermion excitation); (2) one fermion is removed from the Fermi sea (hole excitation); (3) one antifermion is added (antifermion excitation, which can be considered as a hole in the Dirac sea); (4) one boson is added.

Excitations fall into two classes according to their energy : hard excitations with energies of order μ , and soft excitations with energies of order $e\mu$. Hard excitations have the same dispersion relation as free particles, i.e. $E = p$ (recall that all masses are zero), up to perturbative corrections of order $e^2\mu$: they are weakly perturbed by the medium. On the other hand, soft excitations, with energies of order $e\mu$, have a collective nature, and their dispersion relation is strongly modified by the medium (see Appendix A). As in non-relativistic plasmas, the dispersion relation of soft photons consists of two branches [16]: a longitudinal branch corresponding to collective charge oscillations, named “plasmons” in classical plasmas, and a transverse branch corresponding to electromagnetic oscillations. Their wavefunction has a collective component which is a coherent superposition of hole-particle states. Soft gluons have the same dispersion relation as soft photons [17], while soft Yukawa bosons simply have the dispersion relation of a massive particle, with mass $\sim e\mu$. Soft fermions have no counterpart in the nonrelativistic world. Their wavefunction, as for soft photons,

has a collective component which is a coherent superposition of hole–photon states [14]. Their dispersion relation is the same for the three interactions considered here [18,19].

In this paper, we compute to leading order in e the lifetimes of hard one-particle excitations in the presence of the three interactions listed above. The excitation modes are damped as a result of collisions with the fermions of the Fermi sea. For fermion or hole excitations, the only collisional process to leading order in e is elastic (Møller) scattering $ff \rightarrow ff$. For an antifermion, two processes may contribute, namely elastic (Bhabha) scattering $\bar{f}f \rightarrow \bar{f}f$ and pair annihilation $\bar{f}f \rightarrow bb$. For a boson, the only process is elastic (Compton) scattering $bf \rightarrow bf$.

The damping of soft excitations is more complex: even to leading order in e , it involves other processes such as bremsstrahlung $ff \rightarrow ffb$ for a soft hole, or $\bar{f}ff \rightarrow bf$ for a soft antifermion. These calculations will be presented in a forthcoming publication [20].

In a perturbative regime where the coupling constant is small, $e \ll 1$, all the hard excitations have damping rates much smaller (at least by a power of e^3 , as we shall see) than their frequencies, which means that they are well-defined quasiparticles. On the other hand, when studying the non-relativistic electron gas in metals at room temperature [21], the effective couplings are strong: only fermionic excitations very close to the Fermi level have a long lifetime and can be called quasiparticles. The quasiparticles are involved for instance in the calculation of the specific heat at low temperature. The lifetime of fermionic excitations close the Fermi surface will also be studied here in the ultrarelativistic limit, and it will be shown that it becomes infinite at the Fermi surface.

Scattering processes fall into two classes according to the deflection angle. Large scattering angles correspond to hard exchanged quanta: then, as recalled above, medium corrections are small and the amplitude of the process is the same as in the vacuum. On the other hand, if a hard particle of momentum $\sim \mu$ is deflected by a small angle of order e , the exchanged quantum has a soft momentum of order $e\mu$, for which medium corrections become important. Depending on the interaction and on the type of excitation considered, the dominant contribution to the damping rate may come either from processes with large

scattering angles, or from processes with small scattering angles, or from both. This will be explained in section II, where we briefly discuss qualitatively the various physical mechanisms at work and the resulting orders of magnitude of damping rates. In section III, we present the formalism used to calculate the contributions from scattering at large and small angles. Both are computed as phase space integrals of elementary scattering processes. The relation to the field theoretical approach is outlined in Appendix B. Our results, i.e. the lifetimes of hard excitations for the various interactions considered, are given in section IV. They are compared and discussed in section V.

II. ORDERS OF MAGNITUDE

The damping rate Γ of a hard excitation, i.e. the probability per unit time that it undergoes a collision, may be of order $e^4\mu$, $e^4\mu \ln(1/e)$ or $e^3\mu$, depending on the type of excitation and on the interaction. Let us see how this occurs:

The number of collisions per unit time is of order $\Gamma \sim \sigma n v$ where σ is the scattering cross section, n the density of scatterers and v the relative velocity. For massless particles, $v = 1$. The cross section of a $2 \rightarrow 2$ scattering process between massless particles is, for dimensional reasons, of order $\sigma \sim e^4/E^2$, where E is the energy of the particles, which are of order μ here. The density of particles per unit volume in the Fermi sea is of order $n \sim \mu^3$. One then obtains $\Gamma \sim e^4\mu$. This holds when all the elementary $2 \rightarrow 2$ scattering processes involved in the damping have a finite cross section. This is the case for fermion–fermion scattering mediated by a massless scalar in the Yukawa theory (section IV A).

This simple picture is modified by the infrared divergences which frequently occur in massless theories, and which makes the total cross section σ infinite in the vacuum. The most familiar case is the exchange of a gauge boson, which gives the interaction an infinite range: it is well-known that in the vacuum, the differential cross section for Rutherford (or Mott) scattering diverges at small deviation angles θ like $d\sigma/d\Omega \propto 1/\theta^4$, thus σ diverges like $1/\theta^2$. But in a plasma, medium effects come into play: due to the screening of the

electric charge, the interaction potential decreases exponentially for distances larger than the Debye screening length $r_D \sim 1/e\mu$. This causes a saturation of the differential cross section for momentum transfers $q < r_D^{-1} \sim e\mu$, i.e. for scattering angles $\theta < \theta_{\min} \sim e$. The total cross section is therefore of order $\sigma \sim e^4/\mu^2\theta_{\min}^2 \sim e^2/\mu^2$. Now, for small momentum transfers of order $e\mu$, the density of scatterers is no longer $n \sim \mu^3$: because of Pauli blocking, the outgoing electron must have an energy larger than the Fermi energy μ , and only the electrons just below the Fermi surface can contribute, within an interval $\sim e\mu$. Their density is $n \sim e\mu^3$, and one finally obtains $\Gamma \sim \sigma n \sim e^3\mu$ in this case. This holds as soon as a gauge boson is exchanged in the scattering process. This is the case for the fermion and antifermion damping rates in QED and QCD (section IV C), as well as for the gluon damping rate, dominated to leading order by soft gluon exchange via the non-abelian three gluon vertex (section IV E). Note that the screening argument does not apply strictly to magnetic interactions, since static magnetic fields, unlike electric fields, are not screened. However, dynamical screening occurs and kills the infrared divergence. In this respect, the situation is very different at high temperature, where damping rates are of order e^2T and logarithmically infrared divergent in the (resummed) one-loop approximation [4,5]. The essential difference lies in Pauli blocking: at zero temperature, processes in which a boson with energy $\omega \sim e\mu$ is exchanged have a phase space proportional to ω , whereas at high temperature, phase space is proportional to T . This factor ω both contributes a factor e and kills the divergence at $\omega = 0$.

Other infrared divergences arise when the fermion has zero mass. Unlike the previous ones, they are peculiar to ultrarelativistic plasmas. They come into play in processes where the exchanged particle is a fermion, such as pair annihilation and Compton scattering. The vacuum differential cross section diverges for small scattering angles, which correspond to processes in which fermions “turn” into bosons and vice-versa, keeping almost the same momentum. Here, the divergence is in $1/\theta^2$ instead of $1/\theta^4$, so that the total cross section diverges like $\ln \theta$. This divergence is also cured by collective effects, which become important when the momentum transfer is of order $e\mu$. Following the same reasoning as in the previous

case, the total cross section is of order $\sigma = e^4 \ln(1/e)/\mu^2$. For an annihilation process, there is no Pauli blocking in the final state, and the density of scatterers is of order $n \sim \mu^3$, which leads to a damping rate $\Gamma \sim e^4 \ln(1/e)\mu$. This is the dominant contribution to antifermion damping in a Yukawa theory (section IV B). In the case of Compton scattering, the same reasoning applies only if the boson has an energy larger than the Fermi energy, so that it can turn into a fermion having almost the same momentum. Otherwise, Pauli blocking alone inhibits the infrared divergence and the damping is of order $e^4\mu$ (section IV D).

In the first of the three cases discussed above (with a finite tree-level cross section), processes involving soft exchanged quanta (we refer to them as the “soft contribution” to the damping rate) are subleading, because the corresponding phase space (the density of scatterers) is smaller by a factor e than for hard exchanged quanta. On the contrary, it is dominant in the second case (the exchange of a massless boson), because the corresponding cross section is larger by a factor $1/e^2$ than for hard transfer momenta, which compensates for the factor e from phase space. The hard contribution is subleading in this case. Finally, in the third case (the exchange of a massless fermion), both hard and soft contribution are of equal magnitude, and both must be calculated. We separate in the actual computation the hard and soft scales for the exchanged momenta by introducing an arbitrary IR (resp. UV) momentum cutoff q_* in the hard (resp. soft) contribution. The cutoff q_* is chosen at an intermediate scale, $e\mu \ll q_* \ll \mu$. Such a scale separation is well defined in the small coupling limit $e \ll 1$. For $q > q_*$ (hard contribution), collective effects are negligible since $q \gg e\mu$, and the damping rate can be calculated using the same scattering amplitudes as in the vacuum. For $q < q_*$ (soft contribution), medium effects must be taken into account, we will see in section III B that the kinematics is simplified by the fact that the exchanged quantum is much softer than the incoming particle, $q \ll E \sim \mu$. In the region of the cut-off, both approximations are compatible, so that the total damping rate, which is the sum of both contributions, does not depend on the particular value of q_* chosen [9]. A final remark: in all cases, processes involving soft external particles, either incoming or outgoing, are subleading because the associated phase space is small. Thus, the external legs in the

processes considered in this paper will always be hard. The situation is different, of course, when studying the damping of soft excitations [20], where at least the incoming particle is soft.

III. GENERAL ANALYSIS

We now explain how the hard and soft contributions to the damping rate are actually calculated. The incoming and outgoing particles are always hard, and their dispersion relation is always given by $E = p \sim \mu$. When the transfer momenta are also hard, the damping rate is computed from tree diagrams by integration over phase space (section III A). For soft momentum transfers, the intermediate propagator must be resummed [11]. We shall see that the corresponding contribution to the damping rate is most simply calculated as the probability to emit a soft, off-shell, quantum (section III B). This probability emission effectively takes the $2 \rightarrow 2$ scattering processes into account.

A. Hard sector contribution

We shall consider $2 \rightarrow 2$ elementary processes in which an incoming particle of momentum \mathbf{p} (fermion above the Fermi level, antifermion or boson) is added to the system and scatters on a particle of the Fermi sea with momentum \mathbf{k} , $k < \mu$. We denote by \mathbf{p} and \mathbf{k} (resp. \mathbf{p}' and \mathbf{k}') the momenta of the incoming (outgoing) particles. If the excitation under study is a hole in the Fermi sea, incoming and outgoing particles must be interchanged.

The contribution of this process to the damping rate of the added particle is calculated as the total transition rate, integrated over the available phase space. In the case of fermion–fermion scattering, for instance, one obtains

$$\Gamma_h(p) = \frac{1}{8p} \int d\tau_{p'} d\tau_k d\tau_{k'} \overline{|M|^2} (2\pi)^4 \delta^4(p + k - p' - k'). \quad (1)$$

We have included one factor $1/2$ for the identity of the final states, and one for the average over the initial spin states. $\overline{|M|^2}$ is the matrix element squared computed with the usual

Feynman rules and summed over the fermion spin states. The Lorentz invariant phase space volume is $d\tau_k = d^3k/2k(2\pi)^3$. In eq.(1), phase space is limited by the Pauli exclusion principle: the two outgoing electrons are on energy levels above the Fermi surface ($p', k' > \mu$). Similar formulas hold for other processes.

The phase space integral is easily carried out if an appropriate choice of kinematic variables is made: there are 9 integration variables, and 4 constraints, hence 5 degrees of freedom. Since the integrand is invariant under a simultaneous rotation of \mathbf{p}' , \mathbf{k} and \mathbf{k}' about the direction of \mathbf{p} , by integrating over this angle only 4 degrees of freedom remain. At this point, it is convenient to introduce the 4-momentum transferred by the incoming particle to the plasma:

$$\begin{aligned}\omega &\equiv k' - k = p - p', \\ \mathbf{q} &\equiv \mathbf{k}' - \mathbf{k} = \mathbf{p} - \mathbf{p}'.\end{aligned}\tag{2}$$

We choose 3 variables as k , ω and $q \equiv |\mathbf{q}|$. Note that k and ω fix the energy of the incoming and outgoing particles, while q fixes the angle between \mathbf{k} and \mathbf{k}' . The fourth degree of freedom corresponds to the angle between the plane spanned by $(\mathbf{p}, \mathbf{p}')$ and the plane spanned by $(\mathbf{k}, \mathbf{k}')$ or, equivalently, to the azimuthal angle ϕ of \mathbf{k} around \mathbf{q} . With these variables, eq.(1) becomes

$$\Gamma_h(p) = \frac{1}{512\pi^3 p^2} \int dk d\omega dq \left\langle \overline{|M|^2} \right\rangle \tag{3}$$

where the brackets $\langle \rangle$ denote an average over the azimuthal angle ϕ .

The integration limits on q are easily derived from the definition, eq.(2):

$$|\omega| < q < \min(k' + k, p' + p) = \min(2k + \omega, 2p - \omega). \tag{4}$$

Since the scattered fermion belongs to the Fermi sea, we have the constraint $k < \mu$. Depending on whether or not the outgoing particles are electrons, additional constraints on k and ω may result from the Pauli blocking conditions: $k' = k + \omega > \mu$ and/or $p' = p - \omega > \mu$. Together with eq.(4), these conditions completely specify the integration domain in eq.(3).

If all the particles involved in the scattering process are hard (including the exchanged one), the matrix element is the same as in the vacuum, to leading order in the coupling constant e . Then $\overline{|M|^2}$ is Lorentz invariant and can be expressed as a function of the three Mandelstam variables $s = (p+k)^2$, $t = (p-p')^2$, $u = (p-k')^2$. Depending on the theory considered (Yukawa coupling, QED or QCD) and the scattering processes, three different situations occur:

(1) The squared matrix element $\overline{|M|^2}$ is independent of s , t and u . This is the case of fermion–fermion scattering (our example in eq.(1)) in a theory where massless fermions interact through a massless scalar field ϕ , with a Yukawa coupling $e\bar{\psi}\psi\phi$. In this case (see section IV A),

$$\overline{|M|^2} = 12e^4. \quad (5)$$

The integration over the remaining variables in eq.(3) is straightforward, and gives a result of order $e^4\mu$ for p of order μ (see section IV A), in agreement with our discussion in section II. In this case, the soft contribution is subleading and therefore neglected.

(2) The squared matrix element $\overline{|M|^2}$ contains a term like u/t . For instance, for fermions coupled to a scalar field through a Yukawa interaction, the matrix element of e^+e^- annihilation into two bosons is

$$\overline{|M|^2} = 2e^4 \left(\frac{u}{t} + \frac{t}{u} - 2 \right), \quad (6)$$

The phase space integral is evaluated as follows. The first and second term in eq.(6) give equal contributions to the damping rate, since exchanging t and u amounts to exchanging the two outgoing particles. We can thus compute the damping rate using $\overline{|M|^2} = 4e^4(u/t - 1)$.

From the definition of t and eq.(2), one immediately gets

$$t = \omega^2 - q^2. \quad (7)$$

We must then average $u = 2(\mathbf{p} \cdot \mathbf{k}' - pk')$ over the azimuthal angle ϕ between \mathbf{k} and \mathbf{q} . This is easily done by first decomposing \mathbf{p} and \mathbf{k}' into longitudinal and transverse components

with respect to \mathbf{q} . Averaging over ϕ , one gets $\langle \mathbf{p} \cdot \mathbf{k}' \rangle = (\mathbf{p} \cdot \mathbf{q})(\mathbf{k}' \cdot \mathbf{q})/q^2$. From eq.(2), one obtains $\mathbf{p} \cdot \mathbf{q} = \omega p + (q^2 - \omega^2)/2$ and $\mathbf{k}' \cdot \mathbf{q} = \omega k + (q^2 + \omega^2)/2$. A simple calculation gives then

$$\langle u \rangle = \frac{\omega^2 - q^2}{2q^2} \left[(2k + \omega)(2p - \omega) - q^2 \right]. \quad (8)$$

The collinear divergence at $\omega = \pm q$ cancels out in the ratio $\langle u/t \rangle$, but after integrating over ω , a logarithmic infrared divergence in the momentum transfer q appears: for small q -momenta, the constraint (4) reduces to $|\omega| < q$ and the phase space integral in eq.(3) is approximately evaluated as

$$\int_{q_*} dq \int_{-q}^q d\omega \int_0^\mu dk \sim \int_{q_*} 2qdq \int_0^\mu dk, \quad (9)$$

while the average matrix element from eq.(8) becomes, in the limit $q \ll p$, $\langle \overline{|M|^2} \rangle \simeq 4e^4 \langle u/t \rangle \simeq 8e^4 kp/q^2$. We thus obtain for the small q -contribution to the damping rate

$$\Gamma_h(p) \simeq \frac{e^4}{32\pi^3 p} \int_0^\mu kdk \int_{q_*} \frac{dq}{q} \simeq \frac{e^4}{64\pi^3} \frac{\mu^2}{p} \log \frac{\mu}{q_*}, \quad (10)$$

where q_* is an IR cutoff introduced by hand. The whole range (hard and soft) of momentum transfer is thus relevant to leading order and upon adding the soft contribution, the final result is of order $e^4 \mu \log 1/e$ (see sections IV B and IV D), as expected from section II.

(3) The squared matrix element contains a stronger divergence like $(u/t)^2$. This is the case of electron-electron scattering (our example of eq.(1)) in QED, where $\overline{|M|^2}$ is given by the Møller formula:

$$\overline{|M|^2} = 16e^4 \left(\frac{u}{t} + \frac{t}{u} + 1 \right)^2. \quad (11)$$

This diverges for small q like $e^4 \mu^4/q^4$. As to the phase space integral, it differs from the previous case due to Pauli blocking, which imposes the additional constraint $k' = k + \omega > \mu$. Thus eq.(9) is replaced by

$$\int_{q_*} dq \int_0^q d\omega \int_{\mu-\omega}^\mu dk \sim \frac{1}{2} \int_{q_*} q^2 dq. \quad (12)$$

Multiplying by the matrix element and integrating over q , one finds that the damping rate diverges like $1/q_*$: the divergence is linear instead of logarithmic. The scattering process is dominated by soft momentum transfers, and the hard sector contribution can be neglected to leading order. As explained in section II, screening phenomena provide an effective cut-off of order $e\mu$, so that the damping rate is of order $e^3\mu$.

B. Soft sector contribution

When the momentum transfer of a scattering process is of order $e\mu$, one must correct the interaction for medium effects, whose contribution become of the same order as the bare propagator itself. Consider for example electron–electron scattering in QED. The interaction between two charges is screened at large distances by the electrons in the plasma and the bare photon propagator must be replaced by the resummed propagator given in Appendix A. The damping rate is then evaluated as a collision integral similar to eq.(1), however with a screened interaction. As we shall now explain, it can also be cast into a much simpler form, as the transition rate of the process depicted in Fig.1 (left), where a hard electron of momentum p emits of a soft virtual photon.

As shown in Appendix B, the contribution to the damping rate of the collision process with a bare interaction is equal to the imaginary part of the self–energy diagram depicted in Fig.2. This is a consequence of cutting rules (see for example [22]), which state that the imaginary part of a self–energy diagram is the square of the transition rates of the various physical processes obtained by cutting the electron self–energy diagram in all possible ways. To go from the bare interaction to a screened interaction, one needs to take into account all the bubble diagram insertions in the photon line. Only part of the bubble insertions are of the same order as the inverse propagator: these are terms corresponding to coupling the exchanged photon with intermediate hard electron–hard hole states; electron–positron states contribute to higher order only. The dominant contribution is included in a resummed photon propagator depicted by a blob (see Fig.1 and appendix A). Taking the imaginary

part of the corresponding self-energy diagram amounts then to consider the process depicted on the left of Fig.1.

As we shall see, all the soft contributions to damping rates can be calculated by evaluating transition rates of processes analogous to the one depicted in Fig.1: a hard particle with momentum p emits or absorbs a virtual soft particle with momentum q and scatters into a hard particle on mass shell, with momentum p' . The damping rate $\Gamma(p)$ can now be evaluated from Fermi's Golden Rule, as in eq.(1), but with some important modifications. First the soft particle is off-shell (spacelike): it reflects the fact that the actual physical process is (in the example taken above) electron-electron scattering, not "electron decay". Second, the soft energy ω and momentum q are no longer related by a dispersion relation. Instead, a whole range of values are allowed and weighted by a spectral distribution whose actual form is derived from the screening corrections. Note however that phase space is limited by the same statistical constraints as if the soft, off-shell, particle were a real (vs. virtual) incoming or outgoing particle state. The damping rate takes then the following form:

$$\begin{aligned}\Gamma_s(p) &= \frac{1}{2p} \int \frac{d^4q}{(2\pi)^4} \rho(q) \frac{d^4p'}{(2\pi)^4} 2\pi\delta(p'^2) (2\pi)^4\delta^4(p' + q - p) \overline{|M|^2}, \\ &= \frac{1}{2p} \int \frac{d^4q}{(2\pi)^4} \rho(q) 2\pi\delta((p - q)^2) \overline{|M|^2}.\end{aligned}\quad (13)$$

In this expression, $\rho(q)$ denotes the spectral function of the soft particle. The spectral function of the outgoing hard particles is simply $2\pi\delta(p'^2)$. M denotes the matrix element of the transition on the left of Fig.1. A summation over final spins is implicit in eq.(13).

In the limit where q is much softer than p , $(p - q)^2 = -2p(\omega - q \cos \theta)$, where θ is the angle between \mathbf{q} and \mathbf{p} . Thus the condition that the outgoing hard particle is on its mass shell, $(p - q)^2 = 0$ reduces to $\cos \theta = \omega/q$. Integrating over θ , the previous equation becomes

$$\Gamma_s(p) = \frac{1}{16\pi^2 p^2} \int_0^{q^*} q dq \int_{-q}^q d\omega \rho(\omega, q) \overline{|M|^2}.\quad (14)$$

We have not included in this formula the statistical Bose-Einstein and Fermi-Dirac factors, which depend on the particles involved in the scattering process. They will be specified

later. Note that $\omega > 0$ (resp. $\omega < 0$) corresponds to the emission (resp. absorption) of a soft particle.

It turns out that the matrix element squared $|\overline{M}|^2$ always takes a very simple form. To see this, we turn to the four specific cases we shall need in the next section. The first case is electron–electron (Møller) scattering at low angles (section IV C), which we compute as the emission of an off–shell soft photon by a hard electron (Fig.1). Since there are no photons initially present at $T = 0$, there is no photon absorption, only emission, which implies $\omega > 0$ in eq.(14). An additional restriction on the phase space is that the outgoing electron must be above the Fermi level, which implies $\omega < p - \mu$. The matrix element of the transition is $M = e \bar{u}(p', \lambda') \gamma^\mu u(p, \lambda) \epsilon_\mu(q)$, where $\epsilon_\mu(q)$ is the polarization of the photon. Since $q \ll p$, one can replace $\mathbf{p}' = \mathbf{p} - \mathbf{q}$ by \mathbf{p} in the matrix element. Then, the first factor in M is simply the electric current associated with the incoming electron, which reduces to $J^\mu = e \bar{u}(p, \lambda') \gamma^\mu u(p, \lambda) = 2e p^\mu \delta_{\lambda, \lambda'}$, the Kronecker symbol reflecting the fact that helicity is conserved in the process. We thus obtain $M = 2e p \cdot \epsilon$. Now, in the Coulomb gauge, the spectral function of the soft photon receives a contribution from longitudinal and transverse modes, which are denoted by $\rho_L(q, \omega)$ and $\rho_T(q, \omega)$ respectively (see Appendix A). The longitudinal polarization vector gives a matrix element $|\overline{M_L}|^2 = 4e^2 p^2$. The two transverse polarization vectors $\epsilon_T^\mu(q, \lambda)$ satisfy $\sum_{\lambda=1,2} \epsilon_T^i(q, \lambda) \epsilon_T^j(q, \lambda) = \delta_{ij} - q_i q_j / q^2$ which gives $|\overline{M_T}|^2 = 4e^2 p^2 (1 - \omega^2 / q^2)$. The soft contribution to the damping rate can finally be written as

$$\Gamma_s(p) = \frac{e^2}{4\pi^2} \int_0^{q_*} q dq \int_0^{\min(q, p - \mu)} d\omega \left[\rho_L(\omega, q) + \left(1 - \frac{\omega^2}{q^2}\right) \rho_T(\omega, q) \right]. \quad (15)$$

Since the values of ω that contribute to eq.(15) are of order $e\mu$, the condition $\omega < p - \mu$ can be omitted if $p - \mu \gg e\mu$. Pauli blocking plays a role only in a narrow energy interval of order $e\mu$ around the Fermi energy μ . We shall come back to this case in section IV C. The damping of a hole is calculated in the same manner and leads to the same expression eq.(15), with $p - \mu$ replaced by $\mu - p$.

The process in which a hard positron emits a soft photon, corresponding to Bhabha

scattering at low angles, gives the same result (because the electric current is the same as for an electron, up to a sign). The process in which a hard quark emits a soft gluon is also similar because the color current of the quark has the same structure as its electric current. The result is the same, multiplied by a color factor $4/3$: 8 for the soft gluons, $1/3$ for the average over the quark colors and $1/2$ for the trace of $SU(3)$ generator products.

The second case considered in the next section is gluon Compton scattering at low angles (section IV E). In this regime, only one Feynman diagram contributes to leading order (see the diagram on the left of Fig.3). Following the same steps as in the previous case, this process can be viewed as the emission of a soft gluon by a hard one (see Fig.4). The restriction $\omega > 0$ still applies here since the soft gluon is emitted, not absorbed. On the other hand, there is no restriction on the energy of the outgoing hard gluon. Let us now evaluate the matrix element. As we shall see, it is very similar to the previous one. The three gluon vertex, coupling a hard gluon of color index a , momentum p and polarization ϵ_p^a to a hard and a soft gluon of color indices b and c , momenta p' and q and polarizations $\epsilon_{p'}^b$ and ϵ_q^c respectively, is

$$M = e f^{abc} \left(\epsilon_p^a \cdot \epsilon_{p'}^b (p + p') \cdot \epsilon_q^c + \epsilon_{p'}^b \cdot \epsilon_q^c (-p' + q) \cdot \epsilon_p^a + \epsilon_q^c \cdot \epsilon_p^a (-q - p) \cdot \epsilon_{p'}^b \right), \quad (16)$$

where f^{abc} is the $SU(3)$ structure constant. The hard gluons are on-shell transverse gluons, whose polarization vectors satisfy $\epsilon_p^a \cdot p = \epsilon_{p'}^b \cdot p' = 0$. Therefore, in the limit $q \ll p$, the last two terms in eq.(16) vanish. The remaining term is

$$M = 2 e f^{abc} \left(\epsilon_p^a \cdot \epsilon_{p'}^b \right) \left(p \cdot \epsilon_q^c \right). \quad (17)$$

This can be written in the form $M = J_\mu^c \epsilon_q^{\mu c}$ where J_μ^c is the matrix element of the color current between the initial and final hard gluon. In this form, it is analogous to the matrix element obtained in the previous case, for the emission of a soft photon by a hard electron. The gluon damping rate is therefore the result of eq.(15), multiplied by a factor $3/2$ coming from the color degrees of freedom: 3 for the possible ways of transferring color to the soft gluons, and $1/2$ for the symmetry factor.

It is interesting to note that the transition rate depends on the hard particle only through the associated current. We are in a situation where the hard particle is only slightly perturbed by the soft one: in such a situation, the gauge field behaves essentially as a classical field which couples to the current of the hard particles.

The third case considered corresponds to pair annihilation “at low angles”, in the sense that the outgoing photons have momenta very close to the incoming electron and positron (Fig.5, left). This can be viewed as a process where a hard antifermion “turns” into a hard boson by absorbing a soft fermion or emitting a soft antifermion (see Fig.5, right). Here, both $\omega > 0$ (emission of a soft antifermion) and $\omega < 0$ (absorption of a soft fermion) contribute in eq.(14). Let us compute the matrix element M in a Yukawa theory and in QED. The spectral function of a soft fermion receives contributions from two channels which are labeled by $+$ and $-$ in appendix A. We denote by M_+ and M_- the corresponding matrix elements. With the Yukawa interaction, they read

$$M_{\pm} = e\bar{u}(\mathbf{p}, \lambda)u(\pm\mathbf{q}, \lambda'). \quad (18)$$

Only states with opposite chiralities have non-vanishing matrix elements, which implies $\lambda' = -\lambda$. Using eq.(A7) and the property that $|\phi_{\hat{\mathbf{p}}}^\dagger \phi_{\hat{\mathbf{q}}}| = \cos(\theta/2)$, θ denoting the angle between \mathbf{p} and \mathbf{q} , one easily obtains the result

$$\sum_{\lambda'} |M_{\pm}|^2 = 2e^2 p (q \mp \omega), \quad (19)$$

where we have used the relation $\cos \theta = \omega/q$. The soft contribution to the damping rate can finally be written as

$$\Gamma_s(p) = \frac{e^2}{8\pi^2 p} \int_0^{+\infty} q dq \int_{-q}^q d\omega [(q - \omega)\rho_+(\omega, q) + (q + \omega)\rho_-(\omega, q)]. \quad (20)$$

For QED, eq.(18) must be replaced by

$$M_{\pm} = e\bar{u}(\mathbf{p}, \lambda) \boldsymbol{\epsilon}_T \cdot \boldsymbol{\gamma} u(\pm\mathbf{q}, \lambda'), \quad (21)$$

where $\boldsymbol{\epsilon}_T$ is the polarization vector of the outgoing photon. In the soft limit $q \ll p$, the momentum of the photon is almost equal to \mathbf{p} , so that $\boldsymbol{\epsilon}_T$ is transverse with respect to \mathbf{p} ,

$\epsilon_T \cdot \hat{\mathbf{p}} = 0$. Then, the operator $\epsilon_T \cdot \gamma$ anticommutes both with the chirality operator γ^5 and with the Dirac operator $p\gamma^0 - \mathbf{p} \cdot \gamma$. Thus, it simply changes $\bar{u}(\mathbf{p}, \lambda)$ into $\bar{u}(\mathbf{p}, -\lambda)$, up to a phase. The only difference with the Yukawa interaction is that the chirality λ is conserved. Since the result (19) is independent of λ (by parity symmetry), the result for QED is the same as for the Yukawa interaction, multiplied by a factor 2 to account for the two polarization states of the photon.

Once again, it is interesting to note that two different interactions (Yukawa and QED) give basically the same result: here, it is the fermionic soft field which acts as a classical field (recall that the dispersion relation of soft fermions is the same for both interactions) in which the hard particles move [12].

The fourth and last case corresponds to Compton scattering at low angles with Yukawa or QED interactions (Fig.6, left). This is equivalent to the emission of a soft antifermion (or to the absorption of a soft fermion) by a hard boson (Fig.6, right). Because of Pauli blocking, the outgoing (hard) electron must have an energy $p' > \mu$. Hence there is a soft contribution only if the photon has an energy above, or just below (within an interval of order $e\mu$) the Fermi level μ . The matrix element of the diagram in Fig.6 can be computed in exactly the same way as the one in Fig.5. The resulting soft contribution to the damping rate is still given by eq.(20) for both Yukawa and QED.

IV. DAMPING RATES OF HARD PARTICLES

We now compute explicitly the damping rates of one-particle excitations to leading order in e for the three theories (Yukawa, QED and QCD). We will first study the fermionic excitations, in sections IV A to IV C and then the bosonic excitations, in sections IV D and IV E. For each type of excitation, we show the self-energy diagrams whose imaginary part corresponds to the elementary process under consideration.

A. Fermion in Yukawa's theory

Consider an incoming electron of momentum \mathbf{p} above the Fermi level: $p \geq \mu$. The leading contribution to its damping rate comes from elastic collisions with the electrons in the Fermi sea, which promote an electron of momentum \mathbf{k} above the Fermi sea. In the Yukawa theory, the electron-electron scattering matrix element squared, corresponding to the Feynman diagrams depicted in Fig.7, is a constant: $|\overline{M}|^2 = 12e^4$. Collisions are thus dominated by hard momentum transfers, as discussed in the previous section. The rate Γ is written as the phase space integral of eq.(3), where Fermi statistics imposes the conditions

$$0 < \mu - k < \omega < p - \mu. \quad (22)$$

Using eq.(22), the limits on q given by eqs.(4) reduce to $\omega < q < 2k + \omega$. The integration is straightforward and leads to the expressions

$$\Gamma(p) = \begin{cases} \frac{e^4}{128\pi^3} \frac{\mu^2(3p - 4\mu)}{p^2} & \text{for } p > 2\mu, \\ \frac{e^4}{128\pi^3} \frac{(p - \mu)^2 (4\mu - p)}{p^2} & \text{for } \mu < p < 2\mu. \end{cases} \quad (23)$$

This damping rate corresponds to the imaginary part of the two-loop diagrams displayed in Fig.8. The third two-loop diagram, the rainbow diagram (see Fig.10) does not contribute at zero temperature: its imaginary part corresponds to Compton scattering.

Consider now a hole state (of momentum \mathbf{p} , $p < \mu$), still with a Yukawa interaction. The scattering process is now described in two steps: first an initial vacancy in the Fermi sea is filled by an electron of momentum \mathbf{p}' ; next the energy difference $p' - p$ is transferred to an electron of momentum \mathbf{k}' , which is then extracted out of the Fermi sea. Hence, Fermi statistics imposes for this process the conditions $0 < k', p' < \mu < k$. We define ω and q as in eq.(2). Thus eqs.(3) and (4) are still valid. However, eq.(22) is now replaced by

$$p - \mu < \omega < \mu - k < 0. \quad (24)$$

With these conditions, eq.(4) reduces to $-\omega < q < 2p - \omega$. The phase space integration of eq.(3) gives then

$$\Gamma(p) = \frac{3e^4}{128\pi^3} \frac{(\mu - p)^2}{p}. \quad (25)$$

Near the Fermi surface, the damping rate of fermions and holes vanishes quadratically with the excitation energy $|p - \mu|$. We shall come back to this in section V.

Note that the damping rate diverges for small p . Extrapolating the above formula to the soft domain $p \sim e\mu$ (where our calculation does not apply), one guesses that Γ is of order $e^3\mu$ for a soft excitation, instead of $e^4\mu$ for a hard excitation. A correct calculation shows that it is indeed the case [20].

B. Antifermion in Yukawa's theory

Two collision processes contribute to leading order : Bhabha scattering (Fig.9a) and pair annihilation (Fig.9b).

The first one gives no difficulty. Its matrix element is

$$\overline{|M|^2} = 4e^4, \quad (26)$$

and the phase space integration goes along the same lines as in section IV A, except for the fact that no restriction applies on the final state energy p' . Eq.(22) is therefore replaced by

$$0 < \mu - k < \omega. \quad (27)$$

The contribution of this process to the damping rate is then obtained by integrating eq.(3) using eqs.(4) and (27), and multiplying by a factor of 2 because the final particles are no longer identical:

$$\Gamma_1(p) = \begin{cases} \frac{e^4}{192\pi^3} p & \text{for } p < \mu, \\ \frac{e^4}{192\pi^3} \frac{\mu^2}{p^2} (3p - 2\mu) & \text{for } p > \mu. \end{cases} \quad (28)$$

For pair annihilation, the tree matrix element is given by eq.(6), and we need to include both hard and soft momentum transfers, according to the discussion following this equation. Exchanging t and u amounts to exchanging the two outgoing photons, thus the u/t and t/u terms give identical contributions and $\overline{|M|^2}$ can be replaced by $4e^4(u/t - 1)$. Defining ω and

q as in eq.(2), we can use again eq.(3) to compute the hard contribution to the damping rate. The matrix element averaged over the azimuthal angle ϕ follows immediately from eq.(8). The limits on q are still given by eq.(4), and the only additional restriction from Fermi statistics is $k < \mu$. The integral is logarithmically divergent:

$$\Gamma_{2h}(p) = \frac{e^4 \mu^2}{128\pi^3 p} \left(\log \frac{\mu p}{q_*^2} - \frac{3}{2} \right), \quad (29)$$

where q_* is an IR cutoff for the q -integral. Note that the infrared behavior is in agreement with eq.(10). We must take into account the soft contribution, given by eq.(20), to remove the cutoff [9].

Using the relationship $\rho_+(\omega, q) = \rho_-(-\omega, q)$, the soft contribution given by eq.(20) becomes

$$\Gamma_{2s}(p) = \frac{e^2}{4\pi^2 p} \int_0^{q_*} q dq \int_{-q}^q d\omega (q - \omega) \rho_+(q, \omega), \quad (30)$$

To sum over ω , we first show the following sum rule:

$$\int_{-\infty}^{\infty} d\omega (q - \omega) \rho_+(q, \omega) = 0. \quad (31)$$

Since ρ_+ is the discontinuity of the Green function G_+ on the real axis, the contour integral in eq.(31) is simply the integral of $(q - z)G_+(q, z)$, with z on a contour going parallel and right above the real axis from $-\infty$ to $+\infty$, and coming back right below it from $+\infty$ to $-\infty$. Deforming the contour into a circle of infinite radius, on which $G_+(q, z)$ reduces to the free propagator $[2q(z - q)]^{-1}$, one easily sees that the integral vanishes. With the help of the sum rule of eq.(31), one can then express the contribution from the cut piece ($-q < \omega < q$) of the density ρ_+ in eq.(30) in terms of the pole piece ($|\omega| > q$) of the density ρ_+ :

$$\Gamma_{2s}(p) = \frac{e^2}{4\pi^2 p} \int_0^{q_*} q dq \int_{|\omega|>q} d\omega (\omega - q) 2\pi\delta(2q(\omega - q) - \Sigma_+(q, \omega)). \quad (32)$$

Here, the density ρ_+ has been approximated by $2\pi\delta(G_+^{-1})$ for values of ω close to the quasi-particle energies. Since the mass operator $\Sigma_+(q, \omega)$, given by eq.(A10), depends only on ω/q , it is convenient to change variables from q, ω to $x = \omega/q$ and $y = 2q(\omega - q)$, which gives

$$\Gamma_{2s}(p) = \frac{e^2}{16\pi p} \int \frac{y dx dy}{|x-1|} \delta(y - \Sigma_+(x)). \quad (33)$$

This can be readily integrated over y and then over x . The integration limits are derived from the dispersion relation eq.(A11). For $q \gg m_f$, one peak is at $x \simeq 1 + m_f^2/q^2$ and the other is at $x \simeq -1$. Thus the integral on x extends from $-\infty$ to -1 and from $1 + m_f^2/q_*^2$ to $+\infty$. One gets

$$\Gamma_{2s}(p) = \frac{e^2 m_f^2}{8\pi p} \left[\log \left(\frac{2q_*^2}{m_f^2} \right) - 2 \right]. \quad (34)$$

Replacing m_f by its value given in Appendix A and adding eqs.(29) and (34), the cutoff q_* cancels out. The contribution of pair annihilation to the damping rate is thus

$$\Gamma_2(p) = \Gamma_{2h}(p) + \Gamma_{2s}(p) = \frac{e^4 \mu^2}{128\pi^3 p} \left[\log \left(\frac{2\mu p}{m_f^2} \right) - \frac{7}{2} \right] \quad (35)$$

The total damping rate to order e^4 is the sum of Γ_1 and Γ_2 given by Eqs.(28) and (35). It corresponds to the imaginary part of the self-energy diagrams displayed in Fig.10. The two-loop diagrams give the hard contribution, while the (resummed) one-loop diagram gives the soft contribution.

C. Fermion and antifermion in QED and QCD

We turn now to studying the fermion lifetime in relativistic QED and QCD plasmas. The damping process is electron-electron scattering which is dominated by soft momentum transfers, as explained in section III A. To leading order, the damping rate is therefore given by the soft contribution, eq.(15), with a multiplicative color factor $C_f = 4/3$ for QCD. Introducing the dimensionless quantities $t = q/q_D$, $\varepsilon = |p - \mu|/q_D$, and $x = \omega/q$, one obtains

$$\Gamma(\varepsilon) = C_f \frac{e^2 q_D}{4\pi^2} \int_0^1 dx \int_0^{\varepsilon/x} t^2 dt \left[r_L(t, x) + (1 - x^2) r_T(t, x) \right], \quad (36)$$

with $r_{L,T} = q_D^2 \rho_{L,T}$. We plot the numerical evaluation of $\Gamma(p)$ in Fig.11. We can derive an approximate result in two limits:

1. Far from the Fermi surface, $\varepsilon \gg 1$. As the spectral densities r_L and r_T vanish rapidly for $t \geq 1$, we can extend the upper bound of the t -integral to infinity. One finds

$$\Gamma(p) = 0.057e^2C_fq_D, \quad (37)$$

or

$$\Gamma(p) = \begin{cases} 0.018e^3\mu & \text{for QED,} \\ 0.017\sqrt{N_f}e^3\mu & \text{for QCD with } N_f \text{ flavors.} \end{cases} \quad (38)$$

2. Very close to the Fermi surface, $\varepsilon \ll 1$. The integration over t covers an appreciable range of values for small values of x only. In this limit, the longitudinal and transverse spectral functions behave very differently. Static electric fields are screened at distances larger than q_D^{-1} . As a result, in the limit of small momentum transfer, the longitudinal polarization function, given by eq.(A4), reduces to a constant: $\Pi_L \simeq -q_D^2$. The corresponding spectral function is then

$$r_L = \frac{\pi x}{(t^2 + 1)^2}. \quad (39)$$

The main contribution to the damping rate comes from $q \sim q_D$, or $t \sim 1$, *i.e.* from values of $x \sim \varepsilon$ much smaller than 1. Therefore the integral over x in eq.(36) can be extended to infinity. By changing the order of integration, one finds a contribution to the damping rate of order ε^2

$$\Gamma_L = C_f \frac{e^2 q_D}{4\pi} \int_0^\infty dt \int_0^{\varepsilon/t} dx \frac{xt^2}{(t^2 + 1)^2} + \vartheta(\varepsilon^3) \sim C_f \frac{e^2 q_D}{32} \varepsilon^2 + \vartheta(\varepsilon^3). \quad (40)$$

On the contrary, the transverse polarization function is purely imaginary for $x \ll 1$, because a static magnetic field is not screened. In this limit, eq.(A5) gives $\Pi_T = -i\pi q_D^2 \omega / 4q^3$, and the spectral function is

$$r_T = \frac{\pi x}{2(t^4 + \pi^2(x/4)^2)}. \quad (41)$$

Even though there is no static screening, the term proportional to x^2 in the denominator induces a deviation from the Rutherford $1/q^4$ (*i.e.* $1/t^4$) behavior, which is referred to as

dynamical screening. The main contribution to the damping rate comes from values of t and x such that t^4 and x^2 are of the same order, i.e. such that $q \sim (q_D^2 \omega)^{1/3}$. Since $\omega \ll q_D$, this implies $x \ll 1$: thus the integral over x in eq.(36) can be extended to infinity. Upon introducing the variable $t = u\sqrt{x}/2$ and integrating over x first, one finds

$$C_f \frac{e^2 q_D \varepsilon}{3\pi} \int_0^\infty du \frac{u}{u^4 + \pi^2} + \vartheta(\varepsilon^3) \sim C_f \frac{e^2 q_D}{12\pi} \varepsilon + \vartheta(\varepsilon^3). \quad (42)$$

The damping rate is thus dominated by the transverse contribution and gives

$$\Gamma(p) = \begin{cases} \frac{e^2}{12\pi} |p - \mu| & \text{for QED,} \\ \frac{e^2}{9\pi} |p - \mu| & \text{for QCD with } N_f \text{ flavors.} \end{cases} \quad (43)$$

For the damping rate of a positron or an antiquark, Rutherford scattering has a matrix element varying as $(u/t)^2$ and dominates over pair-annihilation and the s -channel contribution to Bhabha scattering, varying respectively as (u/t) and (u^2/s^2) . The soft sector contribution gives therefore the leading order term, calculated from eq.(15), without any further statistical constraint on the final state energy. The damping rate is then given by the result of eq.(38) for all momenta.

D. Boson in Yukawa's theory and QED

An incident beam (of given central energy) of scalar bosons or photons will undergo a spectral broadening due to the elastic scattering of its quanta with electrons (Compton scattering). The matrix element squared, $\overline{|M|^2}$, corresponding to the diagrams depicted in Fig.12 is related to that of pair annihilation by crossing symmetry. For a Yukawa interaction, one deduces from eq.(6)

$$\overline{|M|^2} = 2e^4 \left(-\frac{u}{s} - \frac{s}{u} + 2 \right), \quad (44)$$

whereas for a hard photon we have, taking into account two final polarization states,

$$\overline{|M|^2} = 4e^4 \left(-\frac{u}{s} - \frac{s}{u} \right). \quad (45)$$

The damping rate computation is similar to the development in the previous section.

To integrate the direct term $-u/s$ over phase space, we define the variables $\omega = p + k = p' + k'$ and $\mathbf{q} = \mathbf{p} + \mathbf{k} = \mathbf{p}' + \mathbf{k}'$, so that $s = \omega^2 - q^2$. Taking k' , ω and q as integration variables, the contribution to the damping rate is given by eq.(3) with k replaced by k' , and multiplied by a factor of 2 because the final particles are not identical. The matrix element $\overline{|M|^2}$ must be averaged over the azimuthal angle of \mathbf{k} around \mathbf{q} . Following the same method as for pair annihilation, we obtain an equation similar to eq.(8):

$$\langle u \rangle = \frac{\omega^2 - q^2}{2q^2} \left[(2k' - \omega)(2p - \omega) - q^2 \right]. \quad (46)$$

The limits on q are $\max(|2p - \omega|, |2k' - \omega|) < q < \omega$, and the constraints from Fermi statistics are $\omega - p < \mu < k'$.

The inverse term $(-s/u)$ is integrated using the variables $\omega = k - p' = k' - p$, $\mathbf{q} = \mathbf{k} - \mathbf{k}' = \mathbf{k}' - \mathbf{p}$ and following the same steps as for the direct term. As discussed at the end of section III B, this leads to a logarithmic divergence if the energy of the incoming photon is larger than the Fermi energy μ , or just below, within an interval of order $e\mu$. In this case, as for pair annihilation we need to introduce a lower cutoff q_* , satisfying the condition $q_* \gg e\mu$.

Adding up the direct and inverse terms, we find for the hard sector contribution to the damping rate of a Yukawa boson

$$\Gamma(p) = \begin{cases} \frac{e^4 p}{192\pi^3} \left[1 - \frac{3\mu^2}{p^2} \log \left(1 - \frac{p^2}{\mu^2} \right) \right] & \text{for } p < \mu \\ \frac{e^4 \mu^2}{64\pi^3 p} \left[3 - \frac{2\mu}{3p} + \log \left(\frac{(p - \mu)p\mu}{(p + \mu)q_*^2} \right) \right] & \text{for } p > \mu \end{cases} \quad (47)$$

and for a photon (QED) we obtain

$$\Gamma(p) = \begin{cases} -\frac{e^4 p}{96\pi^3} \left[1 + \frac{3\mu^2}{p^2} \log \left(1 - \frac{p^2}{\mu^2} \right) \right] & \text{for } p < \mu, \\ \frac{e^4 \mu^2}{32\pi^3 p} \left[1 + \frac{2\mu}{3p} + \log \left(\frac{(p - \mu)p\mu}{(p + \mu)q_*^2} \right) \right] & \text{for } p > \mu \end{cases} \quad (48)$$

The soft contribution to Compton scattering comes from the exchange process of Fig.12 when the intermediate fermion line is soft. We assume for simplicity that $|p - \mu| \gg e\mu$. Then for $p < \mu$, the intermediate fermion line is always hard and the soft contribution is subleading. For $p > \mu$, however, the intermediate fermion state has a soft energy when

the incoming photon (boson) transfers almost all its energy to the outgoing electron. The corresponding soft contribution has already been evaluated in section III B. It takes the same form as the soft contribution for positron annihilation in eq.(30) with an additional factor 2 for the initial electron spins, and with an additional restriction on phase space from Fermi statistics, which requires that $p - \omega > \mu$, as in section IV C. Since ω is of order $e\mu$, this restriction can be ignored as soon as the photon energy is not too close to the Fermi energy, i.e. if $p - \mu \gg e\mu$. If this condition is fulfilled, the damping rate is given by eq.(34) with the additional factor 2 for the initial electron spin, and a factor 1/2 in QED to average over photon helicities. Adding up the hard and soft contributions, we find therefore for the hard Yukawa boson

$$\Gamma(p) = \begin{cases} \frac{e^4 p}{192\pi^3} \left[1 - \frac{3\mu^2}{p^2} \log \left(1 - \frac{p^2}{\mu^2} \right) \right] & \text{for } p < \mu, \\ \frac{e^4 \mu^2}{64\pi^3 p} \left[1 - \frac{2\mu}{3p} + \log \left(\frac{2p\mu(p - \mu)}{m_f^2(p + \mu)} \right) \right] & \text{for } p > \mu, \end{cases} \quad (49)$$

and for a hard photon

$$\Gamma(p) = \begin{cases} -\frac{e^4 p}{96\pi^3} \left[1 + \frac{3\mu^2}{p^2} \log \left(1 - \frac{p^2}{\mu^2} \right) \right] & \text{for } p < \mu, \\ \frac{e^4 \mu^2}{32\pi^3 p} \left[-1 + \frac{2\mu}{3p} + \log \left(\frac{2p\mu(p - \mu)}{m_f^2(p + \mu)} \right) \right] & \text{for } p > \mu. \end{cases} \quad (50)$$

Once again the cutoff q_* has canceled out upon addition of the hard and soft contributions. These results are valid only far from the Fermi surface, i.e. for $|p - \mu| \gg e\mu$. The corresponding self-energy diagrams are displayed in Fig.13.

E. Gluon

Three tree diagrams contribute to Compton scattering of a gluon, they are displayed in Fig.3. The first one has been shown in section III B to yield a contribution of order $e^3\mu$; the contribution from the other ones is subleading and is of the same order in e as in QED, i.e. of order $e^4\mu$ or $e^4\mu \log(1/e)$ (see previous subsection). As discussed in section III B, the damping rate is the same as for the electron (eq.(37)), up to a color factor 3/2:

$$\begin{aligned} \Gamma(p) &= \frac{3}{2} 0.057 e^2 q_D, \\ &= 0.019 \sqrt{N_f} e^3 \mu. \end{aligned} \quad (51)$$

V. DISCUSSION

A first observation is that damping rates of hard particles in a cold ultrarelativistic fermion gas are at least of order e^3 higher than their energy: therefore one-particle excitations are narrow quasiparticle states in the perturbative regime $e \ll 1$, narrower by at least one power of e higher than at high temperature.

For each collision process, we were led to distinguish scattering at large ($\theta \sim 1$) and small ($\theta \sim e$) angles, yielding the hard and soft contributions respectively. The dominant contribution to an excitation damping rate can be hard, or soft, or both, depending on the type of excitation and on the interaction considered. We present in the following table a summary of the orders of magnitude for the different damping rates calculated in this paper.

Leading term in $ \overline{M} ^2/e^4$	Relevant sector	Order of $\Gamma(p)$	Section numbers
1	hard	$e^4\mu$	IV A and IV D
u/t	hard and soft	$e^4\mu \log(1/e)$	IV B and IV D
u^2/t^2	soft	$e^3\mu$	IV C and IV E

With a Yukawa coupling, the damping rate of an electron is completely dominated by the hard contribution, while the soft contribution dominates fermion–fermion scattering in QED and QCD. In terms of self-energy diagrams, the dominant contribution comes from two-loop diagrams in the Yukawa theory, while it comes from a resummed one-loop diagram in QED.

The underlying physics is very different for the hard and soft contributions. The hard contribution simply results from incoherent collisions: the excitation dies off by kicking electrons out of the Fermi sea randomly. By contrast, damping at small scattering angles (the soft contribution) takes place through the creation of coherent oscillations of the charge and current densities. This occurs only when the interaction is mediated by a gauge boson. The underlying classical structure of gauge theories has been outlined in section III B. We have expressed the damping rate resulting from these means field effects as a collision integral for

the scattering process of the initial hard field on the soft virtual field carrying the interaction. Although practical for computational purposes, one should be aware that this formulation is only a convenient way of taking into account the interaction screening effects, static as well as dynamic (Landau damping).

It is interesting to note that scattering at small angles gives rise to a damping rate which is independent of the particle energy, except for electrons or quarks very close to the Fermi surface (see below). By contrast, in a Yukawa theory, the damping rates depend strongly on the energy, as can be seen in Fig.14. Note also that our calculation in gauge theories is valid only for hard excitations. The damping of soft excitations in gauge theories has very different properties: first, it is energy dependent; second, the hard contribution is no longer negligible, but becomes of the same order of magnitude as the soft contribution, yielding a damping rate of order $e^3\mu \log(1/e)$, instead of $e^3\mu$ for hard excitations [20]. Finally, the photon and the scalar boson damping rates show an interesting energy dependence: their damping rates rise steeply near the Fermi energy (see Figs.14 and 15). This phenomenon is characteristic of a relativistic plasma. The gluon damping rate, however, behaves very differently: it is a constant for all momenta; the gluon damping rate is similar to those of charged particles.

Compared to the high temperature, $\mu = 0$ case, an important difference is that there is no particle–antiparticle symmetry. Although the dispersion relations are the same for electrons and positrons, even at finite density [14], it is not the case for the damping rates: in the Yukawa theory, for instance, the latter are of order $e^4\mu$ for electrons and $e^4\mu \log(1/e)$ for positrons.

Last, we comment on the results of the fermion lifetime close to the Fermi surface for a theory with Yukawa coupling and for QED/QCD. For Yukawa coupling, hard momentum transfers dominate (in this sense the interaction is short–ranged) and the damping rate of an electron close to the Fermi surface is *quadratic* in $|p - \mu|$. For gauge theories (QED or QCD), the longitudinal part of the interaction is screened at low momenta and leads to a *quadratic* width close to the Fermi surface. The dominant term shown in eq.(43) is the

contribution from the transverse piece of the interaction, which is not screened in the static limit, and the width is *linear* in $|p - \mu|$. This correlation between the range of interaction and the electron damping rate close to the Fermi surface is already well-known in the non-relativistic electron gas ([23] and [24]). In particular, our result of eq.(43) is in accordance with the energy dependence of the imaginary part of the electron self-energy derived in [24], for a Fermi velocity $p_F/m = v_F \rightarrow 1$.

ACKNOWLEDGMENTS

After completion of this work, we learned that M. le Bellac and C. Manuel have recently calculated the damping rates of electrons and holes near the Fermi surface in QED and QCD [25]. We have benefited from discussions with a number of people. It is a pleasure to thank J.P. Blaizot and E. Iancu for useful comments on the manuscript as well as G. Baym for helpful remarks. This work has been supported in part by the US National Science Foundation under Grant NSF PHY94-21309.

APPENDIX A: SPECTRAL DENSITIES OF SOFT MODES

1. Soft gauge field

In the Coulomb gauge, rotational invariance allows one to decompose the photon or gluon propagator into a longitudinal (L) and a transverse (T) piece [26]:

$$D^{\mu\nu}(\mathbf{q}, z) = D_L(q, z)\epsilon_L^\mu\epsilon_L^\nu + D_T(q, z)\sum_{\lambda=1,2}\epsilon_T^\mu(\mathbf{q}, \lambda)\epsilon_T^\nu(\mathbf{q}, \lambda) \quad (\text{A1})$$

where $\epsilon_L^\mu = \delta_0^\mu$ and $\epsilon_T^\mu(\mathbf{q}, \lambda)$, $\lambda = 1, 2$, are spacelike unit vectors mutually orthogonal and transverse to \mathbf{q} , therefore satisfying $\sum_{\lambda=1,2}\epsilon_T^i(\mathbf{q}, \lambda)\epsilon_T^j(\mathbf{q}, \lambda) = \delta_{ij} - q_i q_j / \mathbf{q}^2$. For the bare QED or QCD interaction, arising from the exchange of a photon or a gluon, the decomposition of the propagator $D_0^{\mu\nu}(q, z)$ according to eq.(A1) gives

$$D_0^{-1}(q, z) = q^2; \quad D_{0T}^{-1}(q, z) = z^2 - q^2. \quad (\text{A2})$$

For soft momenta $q \sim e\mu$, the propagator is modified by medium effects:

$$D_{\mu\nu}^{-1}(q, z) = D_{0,\mu\nu}^{-1}(q, z) - \Pi_{\mu\nu}^*(q, z). \quad (\text{A3})$$

To leading order in e^2 , the polarization tensor $\Pi_{\mu\nu}^*(q, z)$ is given by bubble diagrams corresponding to the photon (or gluon) coupling to electron–hole (or quark–hole) intermediate states. Decomposing $\Pi_{\mu\nu}^*$ according to eq.(A1), one gets [16,17]:

$$\frac{1}{q_D^2} \Pi_L(q, \omega + i\eta) = -1 + \frac{\omega}{2q} \left[\log \left| \frac{\omega + q}{\omega - q} \right| - i\pi\theta(q^2 - \omega^2) \right], \quad (\text{A4})$$

$$\frac{1}{q_D^2} \Pi_T(q, \omega + i\eta) = \frac{\omega^2}{2q^2} + \frac{\omega(q^2 - \omega^2)}{4q^3} \left[\log \left| \frac{\omega + q}{\omega - q} \right| - i\pi\theta(q^2 - \omega^2) \right], \quad (\text{A5})$$

where q_D is the Debye screening momentum, listed for the different theories under consideration in the following table:

Theory	q_D
QED	$e\mu/\pi$
QCD	$e\mu\sqrt{N_f}/\pi\sqrt{2}$

The resummed propagator obtained from eqs.(A3–A5) is drawn as a photon propagator with a “blob” (see for instance Fig.1).

The spectral density $\rho^{\mu\nu}(\mathbf{q}, \omega) = -2 \operatorname{Im} D^{\mu\nu}(\mathbf{q}, \omega + i\eta)$ can be decomposed, like the propagator in eq.(A1), into longitudinal and transverse pieces, $\rho_{L,T}(q, \omega) = -2 \operatorname{Im} D_{L,T}(q, \omega + i\eta)$. Their expressions are easily obtained from eqs.(A2–A5). For free fields, they reduce to $\rho_{0L}(q, \omega) = 0$, $\rho_{0T}(q, \omega) = 2\pi\delta(\omega^2 - q^2)\Theta(\omega)$: the only peaks are at $\omega = \pm q$ and correspond to transverse photons. For soft momenta, ρ_L and ρ_T are modified by medium effects. The peaks of ρ_T are shifted towards higher values of $|\omega|$, and a peak appears in ρ_L at the values of ω given by $D_{0,L}^{-1}(q, \omega) - \Pi_L(q, \omega) = 0$, corresponding to plasmon modes. Note that the real parts of $D_{L,T}^{-1}(q, \omega)$ are even in ω for fixed q , so that the peaks always appear in pairs of opposite sign $\pm\omega$. In addition to these peaks, the spectral densities have a continuous part for $|\omega| < q$ coming from the imaginary part of the polarization in eqs.(A4–A5), which corresponds physically to Landau damping: waves with $|\omega| < q$ lose their energy by accelerating fermions.

2. Soft fermion

The fermion propagator can be decomposed on a basis of spinors in the following way:

$$G(\mathbf{p}, z) = G_+(p, z) \sum_{\lambda=-1,1} u(\mathbf{p}, \lambda) \bar{u}(\mathbf{p}, \lambda) + G_-(p, z) \sum_{\lambda=-1,1} u(-\mathbf{p}, \lambda) \bar{u}(-\mathbf{p}, \lambda). \quad (\text{A6})$$

In this decomposition, $u(\mathbf{p}, \lambda)$ denotes a solution of the free massless Dirac equation $(p\gamma^0 - \mathbf{p} \cdot \boldsymbol{\gamma})u(\mathbf{p}, \lambda) = 0$ with chirality λ , normalized according to the relation $\sum_{\lambda=-1,1} u(\mathbf{p}, \lambda) \bar{u}(\mathbf{p}, \lambda) = p\gamma^0 - \mathbf{p} \cdot \boldsymbol{\gamma}$. Note that $u(\mathbf{p}, \lambda)$ is a positive energy solution, while $u(-\mathbf{p}, \lambda)$ is the corresponding negative energy solution with the same momentum \mathbf{p} : it corresponds to a positron with momentum $-\mathbf{p}$. An explicit expression of $u(\mathbf{p}, \lambda)$ is most easily obtained in the chiral representation of Dirac matrices:

$$u(\mathbf{p}, +1) = \sqrt{2p} \begin{pmatrix} \phi_{\hat{\mathbf{p}}} \\ 0 \end{pmatrix} \quad u(\mathbf{p}, -1) = \sqrt{2p} \begin{pmatrix} 0 \\ \phi_{-\hat{\mathbf{p}}} \end{pmatrix} \quad (\text{A7})$$

where $\hat{\mathbf{p}} \equiv \mathbf{p}/p$ and $\phi_{\hat{\mathbf{p}}}$ is a two component spinor pointing in the direction of $\hat{\mathbf{p}}$, i.e. satisfying $\boldsymbol{\sigma} \cdot \hat{\mathbf{p}} \phi_{\hat{\mathbf{p}}} = \phi_{\hat{\mathbf{p}}}$, normalized to unity $\phi_{\hat{\mathbf{p}}}^\dagger \phi_{\hat{\mathbf{p}}} = 1$. Note that $\phi_{\hat{\mathbf{p}}} \phi_{\hat{\mathbf{p}}}^\dagger = (1 + \boldsymbol{\sigma} \cdot \hat{\mathbf{p}})/2$

For the free Dirac propagator $G_0^{-1}(\mathbf{p}, z) = z\gamma^0 - \mathbf{p} \cdot \boldsymbol{\gamma}$, the decomposition (A6) gives

$$G_{0\pm}^{-1}(p, z) = 2p(z \mp p). \quad (\text{A8})$$

As expected, the poles of G_+ and G_- are respectively the positive and negative energy solution of the free Dirac equation. For soft momenta $p \sim e\mu$, the fermion propagator is corrected by medium effects:

$$G^{-1}(p, z) = G_0^{-1}(p, z) - \Sigma^*(p, z). \quad (\text{A9})$$

The mass operator $\Sigma^*(p, z)$ can be decomposed according to eq.(A6), so that $G_{\pm}^{-1} = G_{0\pm}^{-1} - \Sigma_{\pm}^*$. To leading order in e^2 , the components Σ_{\pm}^* are given by [18,19]

$$\begin{aligned} \frac{1}{2m_f^2} \Sigma_+(p, \omega + i\eta) &= 1 - \frac{\omega - p}{2p} \left[\log \left| \frac{\omega + p}{\omega - p} \right| - i\pi\theta(p^2 - \omega^2) \right], \\ \Sigma_-(p, \omega + i\eta) &= -\text{Re} \Sigma_+(p, -\omega + i\eta) + i \text{Im} \Sigma_+(p, -\omega + i\eta). \end{aligned} \quad (\text{A10})$$

The quantity m_f is the quasiparticle rest energy and is given in the following table:

Theory	m_f
Yukawa	$e\mu/4\pi$
QED	$e\mu/\pi\sqrt{8}$
QCD	$e\mu/\pi\sqrt{6}$

The spectral density $\rho_F(\mathbf{p}, \omega) = -2 \operatorname{Im} G(\mathbf{p}, \omega + i\eta)$ can be decomposed like the propagator in eq.(A6), with $G_{\pm}(p, z)$ replaced by the corresponding spectral density $\rho_{\pm}(p, \omega) = -2 \operatorname{Im} G_{\pm}(p, \omega + i\eta)$. For a free Dirac field, the spectral density reduces to $\rho_{\pm}(p, \omega) = 2\pi\delta(\omega^2 - p^2)\theta(\pm\omega)$. Medium effects modify the spectral density for soft momenta. The position of the peaks of ρ_+ are the solutions of $G_+^{-1}(p, \omega) = 0$. Using eqs.(A8–A10), one obtains the dispersion relation in terms of the parameter $x \equiv \omega/p$:

$$\frac{p^2}{m_f^2} = \frac{1}{x-1} - \frac{1}{2} \log\left(\frac{x+1}{x-1}\right),$$

$$\omega = px. \quad (\text{A11})$$

There are two peaks for a given p . One with $x > 1$, which corresponds to the bare fermion state slightly shifted by its interaction with the medium. Furthermore, a second peak appears for $x < -1$. It corresponds to a new fermionic excitation called “plasmino” which has no counterpart in non-relativistic plasmas [14]. Finally, ρ_+ has a continuous part in the region $|\omega| < p$, which corresponds to the fermionic analogue of Landau damping. The density ρ_- has the same properties, with ω replaced by $-\omega$.

APPENDIX B: SELF-ENERGY DIAGRAMS AND CUTTING RULES

In this appendix, we show that the electron damping rate $\Gamma(p)$, calculated as a collision rate integrated over phase space, is related to the imaginary part of the electron self-energy through the relation $\Gamma(p) = -2 \operatorname{tr} [\not{p} \operatorname{Im} \Sigma(\mathbf{p}, p + i\eta)] / 4p$ [27].

We first show that the imaginary part of the one-loop resummed diagram depicted in Fig.17 corresponds to the probability to emit a soft quantum (first equality in Fig1). Then

we show the equality displayed in Fig.2, i.e. that the rate of electron–electron scattering, corresponds to the imaginary part of a two–loop self–energy diagram. Note, however, that the interference term between the two Feynman diagrams of electron–electron scattering (Fig.7) is not included here. It corresponds to the imaginary part of another two–loop diagram (Fig.8). Finally, we show that the imaginary part of the one–loop resummed diagram corresponds to electron–electron scattering with a resummed interaction (second equality in Fig.1).

The contribution of the diagram in Fig.17 to the fermion self–energy is given by

$$\Sigma(\mathbf{p}, z_p) = \int \frac{d^3 q}{(2\pi)^3} \int_{-i\infty}^{+i\infty} \frac{dz_q}{2i\pi} (-ie\gamma^\mu) G_0(\mathbf{p} - \mathbf{q}, z_p - z_q) (-ie\gamma^\nu) D_{\mu\nu}(\mathbf{q}, z_q). \quad (\text{B1})$$

In this expression, $z_p = \mu + ix$ with x real, G_0 is the fermion propagator, which coincides with the free propagator (A8) for a hard fermion, and D is the soft photon propagator given by eqs.(A3–A5). We write the internal propagators using the spectral representations:

$$\begin{aligned} D_{\mu\nu}(\mathbf{q}, z_q) &= \int_{-\infty}^{+\infty} \frac{d\omega_q}{2\pi} \frac{\rho_{\mu\nu}(\mathbf{q}, \omega_q)}{z_q - \omega_q}, \\ G_0(\mathbf{p}', z_{p'}) &= \int_{-\infty}^{+\infty} \frac{d\omega_{p'}}{2\pi} \frac{\rho_F(\mathbf{p}', \omega_{p'})}{z_{p'} - \omega_{p'}}, \end{aligned} \quad (\text{B2})$$

with $z_q = ix$ and $z_{p'} = \mu + ix$. A straightforward contour integration gives for the integral over z_q :

$$\int_{-i\infty}^{+i\infty} \frac{dz_q}{2i\pi} \frac{1}{z_q - \omega_q} \frac{1}{z_p - z_q - \omega_{p'}} = -\frac{1 + n(\omega_q) - f(\omega_{p'})}{z_p - \omega_q - \omega_{p'}}, \quad (\text{B3})$$

where we have introduced the Bose–Einstein and Fermi–Dirac distribution functions $n(\omega)$ and $f(\omega)$ which, in the limit $T = 0$, reduce to

$$\begin{aligned} n(\omega) &= \frac{1}{e^{\omega/T} - 1} = \theta(\omega) - 1, \\ f(\omega) &= \frac{1}{e^{(\omega-\mu)/T} + 1} = \theta(\mu - \omega). \end{aligned} \quad (\text{B4})$$

After analytic continuation of z_p to $\omega_p + i\epsilon$, the imaginary part of eq.(B3) becomes

$$\pi\delta(\omega_p - \omega_q - \omega_{p'}) (1 + n(\omega_q) - f(\omega_{p'})). \quad (\text{B5})$$

The imaginary part of the self-energy can thus be obtained from eq.(B1) through replacing the internal propagators by their spectral functions and the Matsubara frequencies z by real frequencies ω , and multiplying by the occupation factor from eq.(B5):

$$-2 \operatorname{Im} \Sigma(\mathbf{p}, \omega_p + i\eta) = \int \frac{d^3 q}{(2\pi)^3} \frac{d\omega_q}{2\pi} (e\gamma^\mu) \rho_F(\mathbf{p} - \mathbf{q}, \omega_p - \omega_q) (e\gamma^\nu) \rho_{\mu\nu}(\mathbf{q}, \omega_q) \times (1 + n(\omega_q) - f(\omega_p - \omega_q)). \quad (\text{B6})$$

Decomposing the spectral functions according to eqs.(A1) and (A6), and taking into account that $\rho_+(\mathbf{p}, \omega) = 2\pi\delta(\omega^2 - p^2)\theta(\omega)$ for a hard fermion (the spectral function is the same as in the vacuum), one obtains

$$-2 \bar{u}(\mathbf{p}, \lambda) \operatorname{Im} \Sigma(\mathbf{p}, p + i\eta) u(\mathbf{p}, \lambda) = \int \frac{d^3 q}{(2\pi)^3} \frac{d\omega_q}{2\pi} 2\pi\delta((p - q)^2) \sum_{j=L,T} \rho_j(q, \omega_q) \sum_{\lambda'} |M_j|^2 \times (1 + n(\omega_q) - f(\omega_p - \omega_q)). \quad (\text{B7})$$

where M_j is the matrix element of the transition process in Fig.1 (left):

$$M_j = \bar{u}(\mathbf{p}', \lambda') (-ie\gamma_\mu) u(\mathbf{p}, \lambda) \epsilon_j^\mu. \quad (\text{B8})$$

Comparing eq.(B7) with eq.(13), one concludes

$$\Gamma(p) = -2 \bar{u}(\mathbf{p}, \lambda) \operatorname{Im} \Sigma(\mathbf{p}, p + i\eta) u(\mathbf{p}, \lambda) / 2p, \quad (\text{B9})$$

$$= -2 \operatorname{tr} [\not{p} \operatorname{Im} \Sigma(\mathbf{p}, p + i\eta)] / 4p. \quad (\text{B10})$$

Note that the occupation factors can be rewritten as

$$1 + n(\omega_q) - f(\omega_{p'}) = (1 + n(\omega_q)) (1 - f(\omega_{p'})) + n(\omega_q) f(\omega_{p'}). \quad (\text{B11})$$

The two terms correspond to the amplitudes for the direct and inverse process in Fig.1 (left). If $\omega_p > \mu$ (particle excitation), only the direct process contributes, when $0 < \omega_q < \omega_p - \mu$. If $\omega_p < \mu$ (hole excitation), on the other hand, only the inverse process contributes, when $\mu - \omega_p < \omega_q < 0$. Note that in this last case, the occupation factor is $n f = -1$; however, the boson spectral function also has an opposite sign for $\omega_q < 0$ (see eqs.(A4-A5) so that the global sign is unchanged.

We now turn to the second step: we show that the imaginary part of the two-loop diagram on the right of Fig.2 corresponds to the rate of electron-electron scattering with the diagram on the left of Fig.2. The contribution of the two-loop diagram to the self-energy is given by a formula analogous to eq.(B1), where D is replaced by a photon line with a fermion loop insertion, i.e. by $D_0 \Pi D_0$, with

$$\Pi^{\mu\nu}(\mathbf{q}, z_q) = \int \frac{d^3 k}{(2\pi)^3} \int_{\mu-i\infty}^{\mu+i\infty} \frac{dz_k}{2i\pi} \text{tr} [G_0(\mathbf{k}, z_k)(e\gamma^\mu)G_0(\mathbf{k} + \mathbf{q}, z_k + z_q)(e\gamma^\nu)] \quad (\text{B12})$$

with z_q on the imaginary axis. Therefore, the imaginary part of the two-loop diagram is given by eq.(B6), in which the boson spectral function $\rho(\mathbf{q}, \omega_q) = -2 \text{Im} D(\mathbf{q}, \omega_q + i\eta)$ is replaced by $-2 \text{Im}(D_0 \Pi D_0)$. Now, the imaginary part of D_0 vanishes because both fermions are on mass shell ($|\omega_p| = p$ and $|\omega_p - \omega_q| = |\mathbf{p} - \mathbf{q}|$), which implies $|\omega| < q$. Thus we can write $\text{Im}(D_0 \Pi D_0) = D_0(\text{Im}\Pi)D_0$. We then follow the same steps as for Σ in eq.(B1). Using the spectral representation to write the internal propagators, the integral over z_k can be calculated easily ($\mathbf{k}' = \mathbf{k} + \mathbf{q}$):

$$\int_{\mu-i\infty}^{\mu+i\infty} \frac{dz_k}{2i\pi} \frac{1}{z_k - \omega_k} \frac{1}{z_k + z_q - \omega_{k'}} = \frac{f(\omega_k) - f(\omega_{k'})}{z_q + \omega_k - \omega_{k'}}. \quad (\text{B13})$$

After analytic continuation of z_q to $\omega_q + i\epsilon$, the imaginary part of this equation becomes

$$\pi\delta(\omega_q - \omega_k - \omega_{k'}) (f(\omega_k) - f(\omega_{k'})). \quad (\text{B14})$$

One thus obtains

$$\begin{aligned} -2 \text{Im} \Pi^{\mu\nu}(\mathbf{q}, \omega_q + i\eta) &= \int \frac{d^3 k}{(2\pi)^3} \frac{d\omega_k}{2\pi} \text{tr} [\rho_F(\mathbf{k}, \omega_k)(e\gamma^\mu)\rho_F(\mathbf{k} + \mathbf{q}, \omega_k + \omega_q)(e\gamma^\nu)] \\ &\quad \times (f(\omega_k) - f(\omega_{k'})). \end{aligned} \quad (\text{B15})$$

Replacing ρ in eq.(B6) by $-2D_0(\text{Im}\Pi)D_0$, using eq.(B15), and decomposing the fermion spectral functions according to eq.(A6), one obtains the rate of electron-electron scattering corresponding to the Feynman diagram in Fig.2:

$$\begin{aligned} \Gamma(p) &= \int \frac{d^3 q}{(2\pi)^3} \int \frac{d\omega_q}{(2\pi)} \int \frac{d^3 k}{(2\pi)^3} \int \frac{d\omega_k}{(2\pi)} (2\pi)\delta((p - q)^2) (2\pi)\delta(k^2) (2\pi)\delta((k + q)^2) \\ &\quad \times |M|^2 (2\pi)\delta(p + k - |\mathbf{p} - \mathbf{q}| - |\mathbf{k} + \mathbf{q}|) (f(\omega_k) - f(\omega_{k'}))(1 + n(\omega_q) - f(\omega_{p'})), \end{aligned} \quad (\text{B16})$$

with $|M|^2 = \sum_{\lambda', \kappa'} |\bar{u}(p', \lambda') \gamma^\mu u(p, \lambda) (1/(\omega_q^2 - q^2)) \bar{u}(k', \kappa') \gamma_\mu u(k, \kappa)|^2$. We only need to check that the product of the phase space factors eq.(B5) and (B14) indeed corresponds to electron–electron scattering. For this purpose, we note that the energy conservation $\omega_q + \omega_k = \omega_{k'}$ implies the following relations between the statistical factors:

$$\begin{aligned} n(\omega_q) (f(\omega_k) - f(\omega_{k'})) &= (1 - f(\omega_k)) f(\omega_{k'}) \\ (1 + n(\omega_q)) (f(\omega_k) - f(\omega_{k'})) &= (1 - f(\omega_{k'})) f(\omega_k) \end{aligned} \quad (\text{B17})$$

Using these equations together with eq.(B11), one obtains immediately the phase space factor under the form

$$(1 - f(\omega_{p'})) f(\omega_k) (1 - f(\omega_{k'})) + f(\omega_{p'}) (1 - f(\omega_k)) f(\omega_{k'}). \quad (\text{B18})$$

The two terms correspond to the amplitudes of the direct and inverse process, as expected.

Finally, we show that the imaginary part of the one loop resummed diagram corresponds to the probability of electron–electron scattering with a screened interaction (second equality in Fig.1). This is a straightforward extension of the previous result. We start from eq.(B6). The spectral function of the resummed photon line, ρ , is given by $\rho = -2\text{Im}D = 2|D|^2(\text{Im}D^{-1})$. Using eq.(A3) and the fact that $\text{Im}D_0^{-1} = 0$, as discussed above, one obtains $\rho = -2|D|^2(\text{Im}\Pi)$. Thus the only difference with the previous case is that the free photon propagator D_0 is replaced by the resummed photon propagator D , which includes the screening effects.

REFERENCES

- [1] J.P. Blaizot, J.-Y. Ollitrault and E. Iancu, *Collective Phenomena in the Quark–Gluon Plasma*, in *Quark–Gluon plasma 2*, Editor R.C. Hwa (World Scientific, 1996), and references therein.
- [2] R.D. Pisarski, Phys. Rev. Lett. **63** (1989) 1129.
- [3] V.V. Lebedev and A.V. Smilga, Phys. Lett. **B253** (1991) 231; Ann. Phys. **202** (1990) 229; Physica **A181** (1992) 187.
- [4] R.D. Pisarski, Phys. Rev. **D47** (1993) 5589.
- [5] H. Heiselberg and C.J. Pethick, Phys. Rev. **D47** (1993) R769.
- [6] S. Peigné, E. Pilon and D. Schiff Z. Phys. **C60** (1993) 455.
- [7] F. Flechsig, H. Schulz and A.K. Rebhan, Phys. Rev. **D52** (1995) 2994.
- [8] E. Braaten, Phys. Rev. Lett. **74** (1995) 2164; E. Braaten and A. Nieto, Phys. Rev. **D51** (1995) 6990.
- [9] E. Braaten and M.H. Thoma, Phys. Rev. **D44** (1991) 2625.; Phys. Rev. **D44** (1991) 1298.
- [10] G. Baym, H. Monien, C.J. Pethick and D.J. Ravenhall, Phys. Rev. Lett. **64** (1990) 1867.
- [11] E. Braaten and R.D. Pisarski, Phys. Rev. Lett. **64** (1990) 1338; Phys. Rev. **D42** (1990) 2156; Nucl. Phys. **B337** (1990) 569.
- [12] J.-P. Blaizot and E. Iancu, Nucl. Phys. **B390** (1993) 589; Phys. Rev. Lett. **70** (1993) 3376.
- [13] J.-P. Blaizot and E. Iancu, Phys. Rev. Lett **76** (1996) 3080; Saclay preprint T96/085, hep-ph 9607303.
- [14] J.-P. Blaizot and J.-Y. Ollitrault, Phys. Rev. **D48** (1993) 1390.

- [15] C. Manuel, Phys. Rev. **D53** (1996) 5866.
- [16] V.P. Silin, Sov. Phys. JETP **11** (1960), 1136.
- [17] H.A. Weldon, Phys. Rev. **D26** (1982) 1394.
- [18] V.V. Klimov, Sov. J. Nucl. Phys. **33** (1981) 934.
- [19] H.A. Weldon, Phys. Rev. **D26** (1982) 2789.
- [20] B. Vanderheyden and J.-Y. Ollitrault, in preparation.
- [21] D. Pines and P. Noziere, *Quantum Fermi Liquids*, Benjamin (New York, 1996)
- [22] L. Kadanoff and G. Baym, “Quantum Statistical Mechanics,” W.A. Benjamin, New-York, 1962; R.L. Kobes and G.W. Semenoff, Nucl. Phys. **B260** (1985) 714; Nucl. Phys. **272** (1986) 329; M. le Bellac, *Thermal field theory*, Cambridge University Press, Cambridge, 1996.
- [23] J.M. Luttinger, Phys. Rev. **121** (1961) 942.
- [24] T. Holstein, R.E. Norton and P. Pincus, Phys. Rev. **B8** (1973) 2649.
- [25] M. le Bellac and C. Manuel, preprint hep-ph/9609369.
- [26] R.D. Pisarski, Physica A **158** (1989) 146.
- [27] H.A. Weldon, Phys. Rev. **D28** (1983) 2007.

FIGURE CAPTIONS

Figure 1: left: Emission of a virtual soft photon by a hard electron, corresponding to small angle e^-e^- scattering. p, λ and p', λ' are the momenta and chiralities of the incoming and outgoing electron, respectively. The direct process is the one depicted, the inverse process corresponds to reading the diagram from right to left, that is the absorption of a photon by an electron of energy p' turning into an electron of energy p . Middle: One-loop self-energy diagram with a resummed photon propagator, indicated by a blob. Right: Diagram for e^-e^- scattering with a screened interaction, equivalent to the diagram in the middle, to leading order.

Figure 2: Left: Tree diagram for e^-e^- scattering. The exchange diagram is negligible when the momentum carried by the internal propagator is soft. Right: Two-loop self-energy diagram. The imaginary part, obtained by cutting the diagram through the fermion loop, corresponds to the amplitude on the left, squared and integrated over phase space.

Figure 3: Tree diagrams of gluon Compton scattering. The first of the three diagrams dominates when the momentum carried by the internal gluon is soft.

Figure 4: Emission of a soft virtual gluon by a hard gluon, representing the contribution of soft momentum transfers to the process depicted in Fig.3.

Figure 5: left: Tree diagram for e^+e^- annihilation. As in Fig.2 (left), the exchange diagram is negligible when the momentum carried by the internal propagator is soft. Right: Emission of a soft virtual positron (or absorption of a soft electron) by a hard positron, representing the contribution of soft momentum transfers to the process on the left.

Figure 6: Left: Leading diagram for Compton scattering in the limit of soft exchanged momenta. Right: Emission of a soft virtual positron (or absorption of a soft electron) by a

hard photon, corresponding to the process on the left.

Figure 7: Tree diagrams for Møller scattering.

Figure 8: Two-loop self-energy diagrams corresponding to the scattering processes depicted in Fig.7. The diagram on the left gives the direct and exchange contribution while the diagram on the right is the interference term.

Figure 9: Tree diagrams for (a) Bhabha scattering and (b) pair annihilation.

Figure 10: Self-energy diagrams corresponding to positron scattering and annihilation. The three two-loop diagrams correspond to the hard contribution: the first diagram corresponds to direct and exchange terms in Bhabha scattering (Fig.9a), the second to direct and exchange terms in pair annihilation (Fig.9b), while the third diagram, which can be cut in two different ways, gives the interference terms of both processes; finally, the one-loop diagram on the right corresponds to the soft contribution.

Figure 11: Tree diagrams for electromagnetic and Yukawa Compton scattering.

Figure 12: Self-energy diagrams corresponding to Compton scattering. The three two-loop diagrams correspond to the hard contribution: the first and second diagrams correspond respectively to the first and second processes in Fig.11, while the third diagram is the interference term; finally, the one-loop diagram on the right corresponds to the soft contribution.

Figure 13: One-loop self-energy diagram contributing to the gluon damping rate through Compton scattering at small angles.

Figure 14: Damping rate of hard one-particle excitations in the Yukawa theory as a function of their momentum p . We have chosen for e the numerical value $e^2/4\pi = 1/137$. Full line: fermion ($p > \mu$, eq.(23)) and hole ($p < \mu$, eq.(25)) excitations; long dashes: antifermion

(eqs.(28) and (35)); short dashes: boson (eq.(49)).

Figure 15: Same as Figure 14 for QED interaction.

Figure 16: Same as Figure 14 for QCD interaction, with $N_f = 2$ flavors. The numerical value of the coupling constant is the same as in Figs. 14 and 15.

Figure 17: One loop resummed diagram contributing to the electron or quark damping rate.

$$\sum_q \left| \begin{array}{c} \text{Diagram with a wavy line and a black dot} \\ p \quad \quad \quad p' \end{array} \right|^2 = -2 \text{Im} \quad \begin{array}{c} \text{Diagram with a wavy line and a black dot} \\ p \quad \quad \quad p' \end{array} = \sum_{k,q} \left| \begin{array}{c} \text{Diagram with a wavy line and a black dot} \\ p \quad \quad \quad p' \end{array} \right|^2$$

Figure 1

$$\sum_{k,q} \left| \begin{array}{c} k \quad \text{---} \quad k' \\ \text{---} \quad \text{---} \quad \text{---} \\ p \quad \text{---} \quad p' \end{array} \right|^2 = -2 \operatorname{Im} \text{ (Diagram)} \quad \text{Diagram: A wavy line with a loop and arrows.}$$

Figure 2

Figure 3

Figure 4

$$\sum_k \left| \begin{array}{c} k \\ p \end{array} \begin{array}{c} \nearrow \text{wavy} \\ \text{dot} \\ \searrow \text{wavy} \end{array} \begin{array}{c} k' \\ p' \end{array} \right|^2 = \left| \begin{array}{c} k \\ p \end{array} \begin{array}{c} \nearrow \text{wavy} \\ \text{dot} \\ \nearrow \text{wavy} \end{array} \begin{array}{c} q, \omega \\ p' \end{array} \right|^2$$

Figure 5

$$\sum_k \left| \begin{array}{c} k \\ p \end{array} \begin{array}{c} \nearrow \text{wavy} \\ \text{dot} \\ \nearrow \text{wavy} \\ \nearrow \text{wavy} \end{array} \begin{array}{c} k' \\ p' \end{array} \right|^2 = \left| \begin{array}{c} k \\ p \end{array} \begin{array}{c} \nearrow \text{wavy} \\ \text{dot} \\ \nearrow \text{wavy} \\ \nearrow \text{wavy} \end{array} \begin{array}{c} q, \omega \\ p' \end{array} \right|^2$$

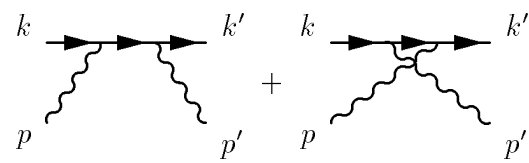
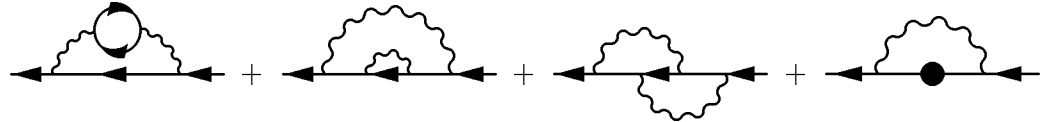
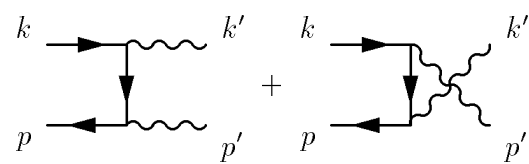
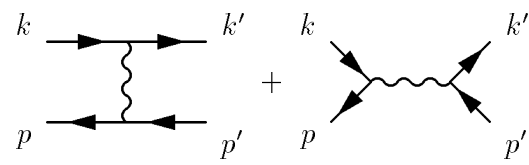
Figure 6

$$\begin{array}{c} k \\ p \end{array} \begin{array}{c} \nearrow \text{wavy} \\ \text{dot} \\ \nearrow \text{wavy} \end{array} \begin{array}{c} k' \\ p' \end{array} + \begin{array}{c} k \\ p \end{array} \begin{array}{c} \nearrow \text{wavy} \\ \text{dot} \\ \nearrow \text{wavy} \\ \nearrow \text{wavy} \end{array} \begin{array}{c} k' \\ p' \end{array}$$

Figure 7

$$\begin{array}{c} \text{wavy loop} \\ \nearrow \text{wavy} \end{array} + \begin{array}{c} \text{wavy loop} \\ \nearrow \text{wavy} \\ \nearrow \text{wavy} \end{array}$$

Figure 8



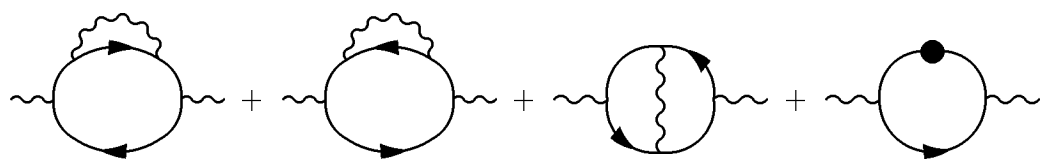


Figure 12

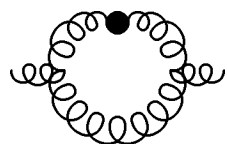


Figure 13

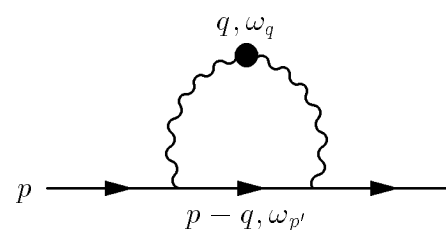


Figure 17

Figure 14

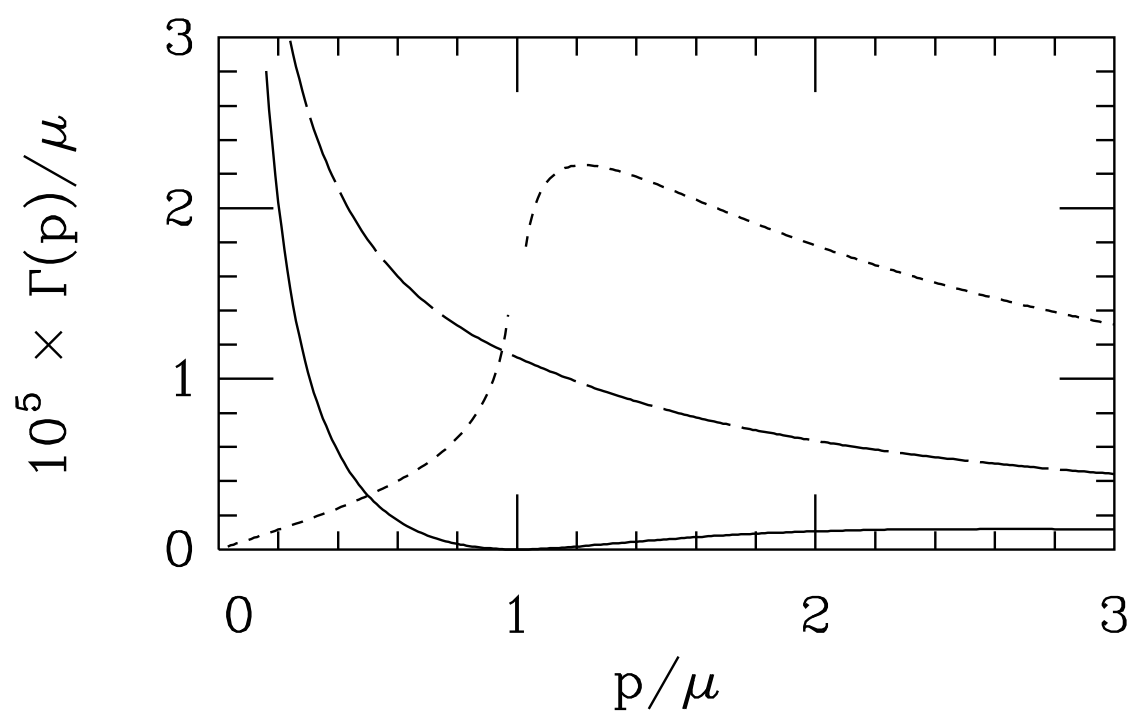


Figure 15

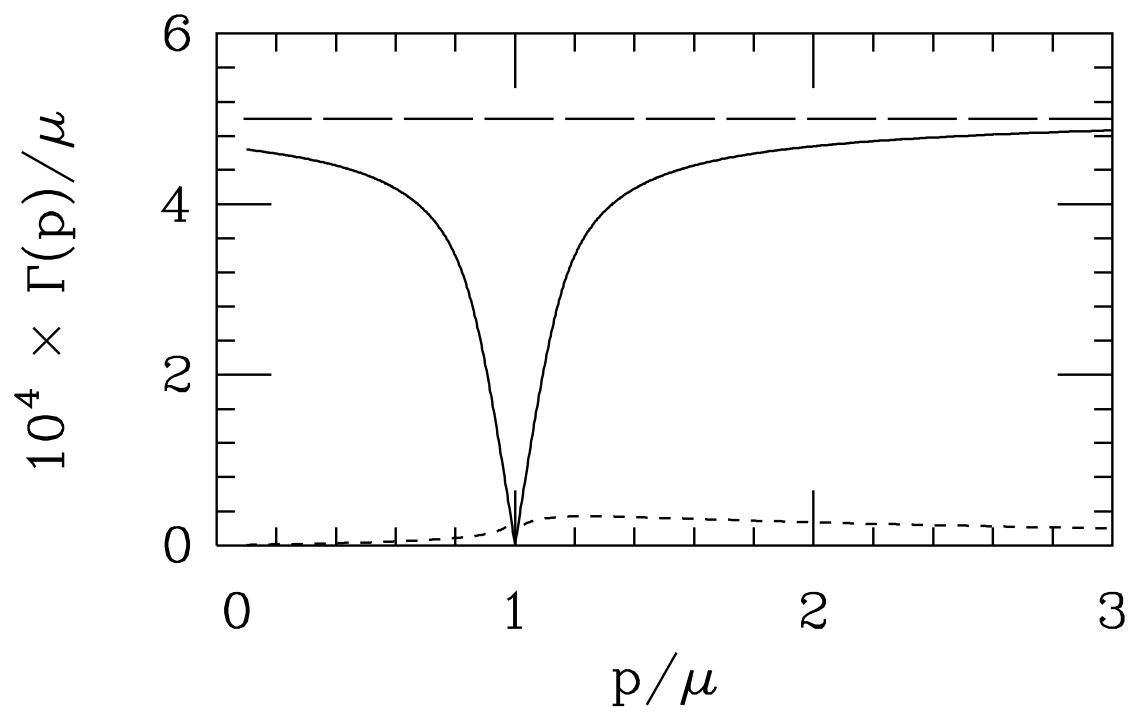


Figure 16

